ELSEVIER

Comput. Methods Appl. Mech. Engrg. 180 (1999) 97–115

Computer methods in applied mechanics and engineering

www.elsevier.com/locate/cma

Variational and momentum preservation aspects of Smooth Particle Hydrodynamic formulations

J. Bonet *, T.-S.L. Lok

Department of Civil Engineering, Institute for Numerical Methods in Engineering, University of Wales Swansea, Singleton Park, Swansea SA2 8PP, UK

Received 20 July 1998

Abstract

This paper presents a new variational framework for various existing Smooth Particle Hydrodynamic (SPH) techniques and presents a new corrected SPH formulation. The linear and angular momentum preserving properties of SPH formulations are also discussed. The paper will show that in general in order to preserve angular momentum, the SPH equations must correctly evaluate the gradient of a linear velocity field. A corrected algorithm that combines kernel correction with gradient correction is presented. The paper will illustrate the theory presented with several examples relating to simple free surface flows.

1. Introduction

Smooth Particle Hydrodynamics (SPH) is a Lagrangian technique whereby the motion of a discrete number of particles of a fluid or a solid is followed in time. Problem variables such as velocity, density, deformation gradient and stresses are obtained from particle values using interpolation functions known as kernels. These techniques were initially developed in astrophysics [1–4] but have now been used extensively for fluid and solid mechanics type of applications [5–16]. A comprehensive review and state of the art description of the method can be found in Refs. [17–25] and is not the purpose of this paper.

Traditionally, there are two different approaches for the evaluation of the material density: by direct interpolation from particle masses; or by time integration of the rate of change of the density given by the continuity equation. In addition, several expressions have been proposed for the evaluation of stress induced interaction forces between particles. All these expressions are derived from the discretization of the same continuum equilibrium equation by making slightly different approximations during the process.

This paper will first present a new formulation for the derivation of the stress forces in terms of an internal energy functional, which will tie together the equations used for the density with the equations employed to express the equilibrium of a particle. This will provide a useful and robust variational framework for the equations used. The paper will then address the momentum preservation properties of the schemes available. It will show that the existence of a variational principle ensures the conservation of linear and angular momentum (in the absence of external forces) on condition that the internal energy is invariant with respect to rigid body motions. Invariance with respect to translations is usually satisfied by most schemes and generally linear momentum is preserved. Rotational invariance, however, requires the

* Corresponding author.
E-mail address: j.bonet@swansea.ac.uk (J. Bonet)

0045-7825/99/$ - see front matter
PII: S0045-7825(99)00051-1

correct evaluation of gradients of linear velocity fields and is more difficult to achieve using simple particle methods. A number of new and existing correction techniques will be presented in order to guarantee the correct evaluation of gradients of linear functions and thereby ensure the preservation of angular momentum.

The applications chosen to illustrate the theory presented relate to the free surface motion of perfect and viscous fluids. The physics of such problems are simple and experimental and analytical comparisons are easily available. A number of examples in this area will be used to discuss the performance of various techniques.

2. Variational framework for SPH algorithms

This section will discuss the possibility of presenting the well-known SPH equations from the point of view of the minimisation of a potential function or energy functional. The advantages of following such a variational approach will become clear in section devoted to momentum preservation where it will be shown that provided that the energy functional is invariant with respect to rigid body motions the formulation will preserve momentum.

2.1. The density equations

Consider a large set of N particles each with a given mass m_b (for $b = 1, \ldots, N$) representing a continuum in motion as shown in Fig. 1. The motion of each particle will be followed by continuously updating its coordinates in a Lagrangian manner in terms of the forces acting on the particle at any time. The evaluation of these forces will inevitably require the knowledge of variables such as the current density of the material being modelled. Typically, the density at a general point $\boldsymbol{x}$, which may or may not coincide with the position of a particle, is interpolated from the masses of surrounding particles in terms of a smoothing or kernel function W as [15–22]:

$$\rho(\boldsymbol{x}) = \sum_{b=1}^{N} m_b W_b(\boldsymbol{x}). \tag{1}$$

The kernel function is scaled to ensure that its integral over the problem domain is one. In this way Eq. (1) can be interpreted as if the discrete mass of each particle is being smoothed over the domain by the function W. Note that, as shown in Fig. 1, kernel functions with a compact support are used for this purpose. Hence the number of particles involved in the above summation is limited to those inside a circle of a given small radius.

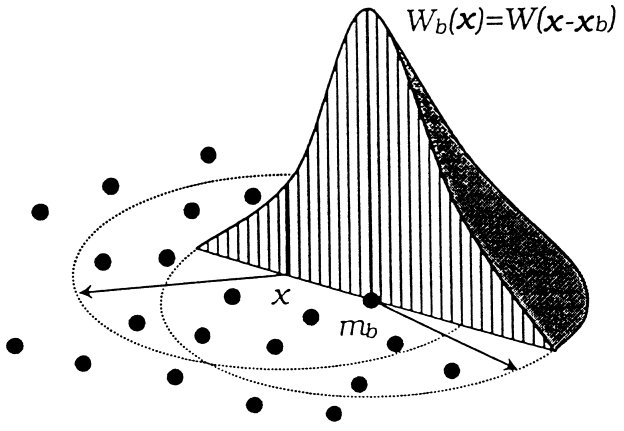

Fig. 1. Particle interpolation and kernel function.

Eq. (1) has been extensively used by several authors for SPH calculations. The resulting interpolation, however, is poor near boundaries where the circle of influence will partially fall outside the problem domain. In an attempt to overcome this difficulty, an alternative formulation for the evaluation of the density is frequently used. This is based on the time integration, using a suitable time stepping scheme, of the continuity equation whereby the material rate of change of the density is related to the divergence of the velocity as

$$\dot{\rho} = -\rho \text{ div } \boldsymbol{v}. \tag{2}$$

Clearly in order to make use of this equation an interpolation of the velocity from particle velocities is required. This is achieved in terms of the kernel function and tributary nodal volumes as [6]

$$\boldsymbol{v}(\boldsymbol{x}) = \sum_{b=1}^{N} V_b \boldsymbol{v}_b W_b(\boldsymbol{x}), \quad V_b = \frac{m_b}{\rho_b}. \tag{3}$$

Differentiation of this equation gives the divergence of the velocity at a particle a as

$$(\text{div } \boldsymbol{v})_a = \sum_{b=1}^{N} V_b (\boldsymbol{v}_b - \boldsymbol{v}_a) \cdot \nabla W_b(\boldsymbol{x}_a). \tag{4}$$

Note that in this equation the term $-\boldsymbol{v}_a$ has been artificially added in order to ensure that the divergence vanishes for a uniform velocity distribution. In addition as the kernel is usually a function of the distance r to its centre, its gradient is evaluated as

$$\nabla W_b(\boldsymbol{x}_a) = \frac{\mathrm{d}W}{\mathrm{d}r} \frac{1}{r_{ab}} (\boldsymbol{x}_a - \boldsymbol{x}_b), \quad r_{ab} = \|\boldsymbol{x}_a - \boldsymbol{x}_b\|. \tag{5}$$

Combining Eqs. (4), (5) and using a suitable time integration of Eq. (2) it is possible to continuously update the density values at each particle.

2.2. The equilibrium equations

The motion of each particle is integrated from the instantaneous acceleration vector $\boldsymbol{a}$, which is governed by Newton's second law:

$$m_a \boldsymbol{a}_a = \boldsymbol{F}_a - \boldsymbol{T}_a, \tag{6}$$

where $\boldsymbol{F}_a$ represents the external forces acting on the particle, such as self-weight, and $\boldsymbol{T}_a$ denotes the equivalent internal forces due to the state of stress inside the material. These forces are typically evaluated from the continuum equilibrium equation div $\boldsymbol{\sigma} + \rho \boldsymbol{f} = \rho \boldsymbol{a}$ using a smoothing or interpolation process similar to that employed for the density. Several results are possible depending on the various approximations made during this process.

For simplicity the case of an isotropic stress tensor $\boldsymbol{\sigma} = p\boldsymbol{I}$ [1] will be considered first. Under such conditions, the most common expressions used in the literature for the internal forces are either,

$$\boldsymbol{T}_a = \sum_{b=1}^{N} m_a m_b \left(\frac{p_a}{\rho_a^2} + \frac{p_b}{\rho_b^2} \right) \nabla W_a(\boldsymbol{x}_b) \tag{7}$$

or, alternatively,

$$\boldsymbol{T}_a = \sum_{b=1}^{N} V_a V_b (p_b \pm p_a) \nabla W_a(\boldsymbol{x}_b). \tag{8}$$

[1] Note that in common with solid mechanics a positive pressure indicates tension throughout this text.

Note that this equation has been used with both + or − signs. The standard derivation of these equations from the local equilibrium equation can be found in Refs. [4,22].

2.3. Internal potential energy

One of the aims of this paper is to show how above equations for the internal forces can be derived from the density equations using a variational approach. For this purpose, let J denote the volume ratio between the initial and current state of the material defined as

$$J = \frac{V}{V^0} = \frac{\rho^0}{\rho}. \tag{9}$$

For an adiabatic process, it is possible to assume the existence of a stored internal energy function $U(J)$ per unit of initial volume of material, from which the pressure p is evaluated as

$$p = \frac{\mathrm{d}U}{\mathrm{d}J}. \tag{10}$$

For instance, for elastic solids $U = (1/2)\kappa(J-1)^2$ whereas for ideal gasses $U = \kappa\rho_0^{\gamma}J^{1-\gamma}$ where κ and γ are material parameter. Similar expressions can be derived for other fluids by integration of the $p(\rho)$ expression.

If the continuum is represented by a large number of particles N distributed over the domain, a total stored energy functional can now be expressed as

$$\Pi(\boldsymbol{x}) = \sum_{a=1}^{N} V_a^0 U(J_a). \tag{11}$$

In the case of an elastic material, for instance, this functional represents the total elastic potential energy of the system. In order to facilitate the derivation of the internal forces from this total potential energy function, the variation, or directional derivative, of a general functional Ψ is defined as [26]

$$D\Psi[\delta\boldsymbol{v}] = \delta\Psi = \left.\frac{\mathrm{d}}{\mathrm{d}\varepsilon}\right|_{\varepsilon=0} \Psi(\boldsymbol{x} + \varepsilon\delta\boldsymbol{v}), \tag{12}$$

where the virtual velocity field $\delta\boldsymbol{v}$ describes a possible movement of the particles. In particular the material time derivative of Ψ is obtained when the virtual velocity coincides with the actual velocity, that is,

$$\dot{\Psi} = D\Psi[\boldsymbol{v}]. \tag{13}$$

With this notation, the variation of Eq. (11) for Π leads to the equivalent internal forces at particle a as

$$D\Pi[\delta\boldsymbol{v}] = \sum_{a=1}^{N} \boldsymbol{T}_a \cdot \delta\boldsymbol{v}_a, \quad \boldsymbol{T}_a = \frac{\partial\Pi}{\partial\boldsymbol{x}_a}. \tag{14}$$

Eq. (14) provides a variational framework for the derivation of the internal forces. It will be shown below that not all the expression used in the literature for the internal forces can be derived from a potential.

2.4. Variational derivation of internal forces

Recalling Eqs. (9) and (10) for U and J, and using the chain rule repeatedly, the directional derivative of Π is obtained as

$$D\Pi[\delta\boldsymbol{v}] = \sum_{a=1}^{N} V_a^0 DU_a[\delta\boldsymbol{v}] = \sum_{a=1}^{N} V_a^0 p_a\left(-\frac{\rho_a^0}{\rho_a^2}\right) D\rho_a[\delta\boldsymbol{v}] = -\sum_{a=1}^{N} m_a\left(\frac{p_a}{\rho_a^2}\right) D\rho_a[\delta\boldsymbol{v}]. \tag{15}$$

The derivative of the density in the equation above will depend on which of the density equations outlined in Section 2.1 is actually used.

2.4.1. Traditional SPH case

Consider first the case where the density is evaluated according to Eq. (1). The variation of the density at a given particle due to a possible virtual movement of the particles is obtained with the help of the chain rule and the use of Eq. (5) for the gradient of the kernel as

$$D\rho_a[\delta \boldsymbol{v}] = \sum_{b=1}^{N} m_b \frac{\mathrm{d}W}{\mathrm{d}r} Dr_{ab}[\delta \boldsymbol{v}] = \sum_{b=1}^{N} m_b \frac{\mathrm{d}W}{\mathrm{d}r} \frac{1}{r_{ab}} (\boldsymbol{x}_a - \boldsymbol{x}_b) \cdot (\delta \boldsymbol{v}_a - \delta \boldsymbol{v}_b)$$
$$= \sum_{b=1}^{N} m_b \nabla W_b(\boldsymbol{x}_a) \cdot (\delta \boldsymbol{v}_a - \delta \boldsymbol{v}_b). \tag{16}$$

Introducing this expression into Eq. (15), rearranging the summations involved and noting that $\nabla W_a(\boldsymbol{x}_b) = -\nabla W_b(\boldsymbol{x}_a)$, gives after simple algebra,

$$D\Pi[\delta \boldsymbol{v}] = \sum_{a,b=1}^{N} m_a m_b \left(\frac{p_a}{\rho_a^2} \right) \nabla W_b(\boldsymbol{x}_a) \cdot (\delta \boldsymbol{v}_b - \delta \boldsymbol{v}_a)$$
$$= \sum_{a=1}^{N} \left[\sum_{b=1}^{N} m_a m_b \left(\frac{p_a}{\rho_a^2} + \frac{p_b}{\rho_b^2} \right) \nabla W_a(\boldsymbol{x}_b) \right] \cdot \delta \boldsymbol{v}_a. \tag{17}$$

By comparison of this expression with Eq. (14), Eq. (7) for the equivalent internal forces is immediately obtained. It transpires therefore, that Eq. (7) for $\boldsymbol{T}_a$ is variationally consistent with Eq. (1) for the density.

2.4.2. Continuity equation case

Consider now the case where the continuity equation (2) is used to update the density. In accordance with Eq. (13), the variation of ρ follows from the time derivative by replacing the real velocity with virtual velocity to give

$$D\rho[\delta \boldsymbol{v}] = -\rho \ \mathrm{div} \ \delta \boldsymbol{v}. \tag{18}$$

Introducing this expression into Eq. (15) and again exploiting the fact that $\nabla W_a(\boldsymbol{x}_b) = -\nabla W_b(\boldsymbol{x}_a)$ gives after some algebra the variation of Π as

$$D\Pi[\delta \boldsymbol{v}] = \sum_{a,b=1}^{N} V_a V_b p_a \nabla W_b(\boldsymbol{x}_a) \cdot (\delta \boldsymbol{v}_b - \delta \boldsymbol{v}_a) = \sum_{a=1}^{N} \left[\sum_{b=1}^{N} V_a V_b (p_a + p_b) \nabla W_a(\boldsymbol{x}_b) \right] \cdot \delta \boldsymbol{v}_a. \tag{19}$$

Comparison of this expression with Eq. (14) yields the internal forces at a given particle as

$$\boldsymbol{T}_a = \sum_{b=1}^{N} V_a V_b (p_b + p_a) \nabla W_a(\boldsymbol{x}_b). \tag{20}$$

Consequently, the version of Eq. (8) that has a positive sign is variationally consistent with the use of Eq. (2) for the density. It will be shown in the applications section that mixing the equations for the density and force in an inconsistent manner leads to poor results.

2.4.3. Shear stresses

So far only isotropic stress tensors have been considered. General materials, however, will exhibit a deviatoric stress component $\boldsymbol{\sigma}'$. In the case of fluids this is due to viscosity whereas for solids more complex constitutive equations possibly involving plasticity can be required. In both cases, the corresponding internal forces can usually be derived from a potential in a manner similar to that shown above for the hydrostatic component. Perhaps the simplest case is that involving fluid viscosity where an additional potential, now a function of particle velocities is postulated in terms of the rate of deformation tensors $\boldsymbol{d}$ as

$$\Pi_\mu(\boldsymbol{v}) = \sum_{a=1}^{N} V_a \psi(\boldsymbol{d}_a), \quad \boldsymbol{d} = \tfrac{1}{2}\left(\nabla \boldsymbol{v} + \nabla \boldsymbol{v}^{\mathrm{T}}\right). \tag{21}$$

In the SPH formulation the velocity gradient is evaluated in a manner similar to Eq. (4) for the divergence to give

$$\nabla \boldsymbol{v}_a = \sum_{b=1}^{N} V_b (\boldsymbol{v}_b - \boldsymbol{v}_a) \otimes \nabla W_b(\boldsymbol{x}_a). \tag{22}$$

The term ψ in Eq. (21) denotes a viscous potential with the physical interpretation of rate of energy dissipated by viscous forces per unit volume. For simple Newtonian fluids it is evaluated in terms of the viscosity μ via the equivalent strain rate as

$$\psi(\boldsymbol{d}) = \tfrac{3}{2}\mu\bar{\varepsilon}^2, \quad \bar{\varepsilon}^2 = \tfrac{2}{3}\boldsymbol{d}' : \boldsymbol{d}', \quad \boldsymbol{d}' = \boldsymbol{d} - \tfrac{1}{3}(\boldsymbol{d} : \boldsymbol{I})\boldsymbol{I}. \tag{23}$$

The directional derivative of the potential shown in Eq. (21) leads, after some algebra, to additional viscous components of the internal forces given by

$$\boldsymbol{T}_a^{\mu} = \sum_{b=1}^{N} V_a V_b (\sigma'_b + \sigma'_a) \nabla W_a(\boldsymbol{x}_b), \quad \sigma' = \frac{\partial \psi}{\partial \boldsymbol{d}} = 2\mu \boldsymbol{d}'. \tag{24}$$

Note that if Eq. (2) is used for the density and, correspondingly, Eq. (20) is employed for the volumetric part of the internal forces, then by adding the viscous component shown in Eq. (24), the total internal forces emerge as

$$\boldsymbol{T}_a = \sum_{b=1}^{N} V_a V_b (\sigma_b + \sigma_a) \nabla W_a(\boldsymbol{x}_b), \quad \sigma = p\boldsymbol{I} + \sigma'. \tag{25}$$

Similar derivations are possible, but lengthier, for elastic and hyperelastic materials.

3. Preservation of momentum

In the absence of external forces, the motion of a continuum – or indeed of a number of particles – must be such that the total linear and angular momentum are preserved. This section will discuss the condition under which the above SPH equations will meet this requirement. The relationship between momentum preservation and the variational formulation presented above will also be discussed.

3.1. Linear and angular momentum

3.1.1. Linear momentum

The total linear momentum of the system of particles is given by

$$\boldsymbol{G} = \sum_{a=1}^{N} m_a \boldsymbol{v}_a. \tag{26}$$

Combining the time derivative of this equation with Newton's second law as given by Eq. (6) in the absence of external forces gives the rate of change of the total linear momentum as

$$\dot{\boldsymbol{G}} = \sum_{a=1}^{N} m_a \boldsymbol{a}_a = -\sum_{a=1}^{N} \boldsymbol{T}_a. \tag{27}$$

Hence the condition for preservation of linear momentum is

$$\sum_{a=1}^{N} \boldsymbol{T}_a = \boldsymbol{0} \tag{28}$$

for any stress distribution.

3.1.2. Angular momentum

Similarly, the total angular momentum of the system with respect to the origin is given by

$$\boldsymbol{H} = \sum_{a=1}^{N} \boldsymbol{x}_a \times m_a \boldsymbol{v}_a. \tag{29}$$

Again time differentiation and the use of the equilibrium equation in the absence of external forces gives

$$\dot{\boldsymbol{H}} = \sum_{a=1}^{N} \boldsymbol{x}_a \times m_a \boldsymbol{a}_a = -\sum_{a=1}^{N} \boldsymbol{x}_a \times \boldsymbol{T}_a. \tag{30}$$

Consequently, angular momentum will be preserved provided that the total moment of the internal forces about the origin vanishes, that is,

$$\sum_{a=1}^{N} \boldsymbol{x}_a \times \boldsymbol{T}_a = \boldsymbol{0}. \tag{31}$$

3.2. Preservation of linear momentum

It is usually quite simple to prove that a particular SPH algorithm satisfies Eq. (28) and hence preserves linear momentum. In general the internal force at particle a can be expressed as the sum of interaction forces between pairs of particles as (see Fig. 2)

$$\boldsymbol{T}_a = \sum_{b=1}^{N} \boldsymbol{T}_{ab}. \tag{32}$$

For instance if the internal forces are given by Eq. (25) then the interaction force is

$$\boldsymbol{T}_{ab} = V_a V_b (\sigma_a + \sigma_b) \nabla W_b(\boldsymbol{x}_a). \tag{33}$$

Given that $\nabla W_a(\boldsymbol{x}_b) = -\nabla W_b(\boldsymbol{x}_a)$, it is clear that $\boldsymbol{T}_{ab} = -\boldsymbol{T}_{ba}$, and consequently the total sum of all interaction pairs will vanish.

If the internal forces can be derived from a potential function, it is also possible to prove that linear momentum is preserved by simply checking that the potential function is invariant with respect to rigid body translations. If this is the case – as it is in all the cases defined above – then the variation of Π due to an arbitrary uniform velocity field $\boldsymbol{v}_0$ will vanish, that is,

$$D\Pi[\boldsymbol{v}_0] = \sum_{a=1}^{N} \boldsymbol{T}_a \cdot \boldsymbol{v}_0 = 0. \tag{34}$$

Given that $\boldsymbol{v}_0$ is arbitrary, Eq. (28) is then necessarily satisfied. The above derivation shows that if the internal forces are derived from a potential that is invariant with respect to rigid body translations, then linear momentum is necessarily preserved.

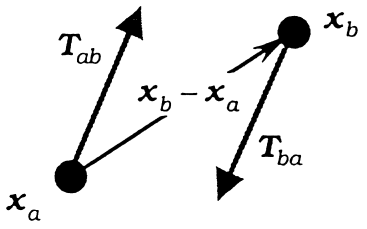

Fig. 2. Interaction forces between two particles.

3.3. Preservation of angular momentum

Although most formulations will preserve linear momentum, the same is not true for angular momentum. As in the previous section the conservation properties of an algorithms can be studied directly or taking advantage of the variational formulation.

3.3.1. Direct method

Consider again the two neighbouring particles shown in Fig. 2. The total moment of the two interacting forces about the origin can be found as

$$\boldsymbol{x}_a \times \boldsymbol{T}_{ab} + \boldsymbol{x}_b \times \boldsymbol{T}_{ba} = -(\boldsymbol{x}_b - \boldsymbol{x}_a) \times \boldsymbol{T}_{ab}, \tag{35}$$

where again the fact that $\boldsymbol{T}_{ab} = -\boldsymbol{T}_{ba}$ has been used. This expression will vanish whenever the interaction force $\boldsymbol{T}_{ab}$ is co-linear with the vector $(\boldsymbol{x}_b - \boldsymbol{x}_a)$ that joins the two particles. Recalling from Eq. (5) that $\nabla W_b(\boldsymbol{x}_a)$ is proportional to $(\boldsymbol{x}_b - \boldsymbol{x}_a)$, it transpires from Eq. (33) that this will be the case only when the stress tensor is isotropic, that is in the absence of shear stresses. In more general situations, therefore, preservation of angular momentum cannot be proved by the above simple procedure and a more general derivation is required.

3.3.2. Variational procedure

It is simple to show that the invariance of the potential energy with respect to rigid body rotations leads to preservation of angular momentum. For this purpose, recall first that a rigid body rotation about the origin is described by a set of velocities given in terms of an angular velocity vector $\delta\boldsymbol{w}$ as

$$\delta\boldsymbol{v}_a = \delta\boldsymbol{w} \times \boldsymbol{x}_a. \tag{36}$$

The invariance of the potential Π with respect to this type of motion implies

$$0 = D\Pi[\delta\boldsymbol{w} \times \boldsymbol{x}_a] = \sum_{a=1}^{N} \boldsymbol{T}_a \cdot (\delta\boldsymbol{w} \times \boldsymbol{x}_a) = \delta\boldsymbol{w} \cdot \sum_{a=1}^{N} \boldsymbol{x}_a \times \boldsymbol{T}_a. \tag{37}$$

Given the arbitrary nature of the angular velocity vector, the preservation condition given by Eq. (31) must be satisfied.

3.3.3. Rotational invariance

In order to examine whether the potential energy function is invariant with respect to rigid body rotations consider again one such motion defined by an angular velocity vector $\boldsymbol{w}$ with components $\left[w_x, w_y, w_z\right]^{\mathrm{T}}$. The velocity vector at any given point is

$$\boldsymbol{v}(\boldsymbol{x}) = \boldsymbol{w} \times \boldsymbol{x} \tag{38}$$

and the true gradient of this velocity filed is found by simple derivation to give

$$\nabla\boldsymbol{v} = \boldsymbol{W}; \quad \boldsymbol{W} = \begin{bmatrix} 0 & -w_z & w_y \\ w_z & 0 & -w_x \\ -w_y & w_x & 0 \end{bmatrix}. \tag{39}$$

Note that the rate of deformation tensor $\boldsymbol{d} = (\nabla\boldsymbol{v} + \nabla\boldsymbol{v}^{\boldsymbol{T}})/2$ and its trace, div$\boldsymbol{v}$, obviously vanish given the skew nature of $\boldsymbol{W}$. Therefore, in the absence of approximations introduced by the discretization, the total potential energy would be independent of rigid body translations. However, if the SPH approximation is used, the gradient of the velocity is evaluated as

$$\nabla\boldsymbol{v}_a = \sum_{b=1}^{N} V_b(\boldsymbol{W}\boldsymbol{x}_b - \boldsymbol{W}\boldsymbol{x}_a) \otimes \nabla W_b(\boldsymbol{x}_a) = \boldsymbol{w}\left(\sum_{b=1}^{N} V_b(\boldsymbol{x}_b - \boldsymbol{x}_a) \otimes \nabla W_b(\boldsymbol{x}_a)\right). \tag{40}$$

Consequently, the correct skew tensor is only obtained if the following matrix condition is satisfied by the gradient of kernel function,

$$\sum_{b=1}^{N} V_b(\boldsymbol{x}_b - \boldsymbol{x}_a) \otimes \nabla W_b(\boldsymbol{x}_a) = \boldsymbol{I} \quad \text{for } a = 1, \ldots, N. \tag{41}$$

Note that satisfying this condition also ensures that the gradient of any linear velocity distribution is correctly evaluated. Unfortunately, standard SPH algorithms do not generally meet this condition and therefore angular momentum will not be preserved. In order to overcome this shortcoming a number of correction techniques can be used.

4. Corrected SPH algorithms

A number of correction techniques have been proposed in the literature with the aim of ensuring that Eq. (41) is satisfied. Some work on the gradient of the kernel directly, whereas others modify the kernel function itself. Both types of techniques will be discussed below before presenting a novel combination of these methods.

4.1. Gradient correction

The simplest correction technique involves modifying the kernel gradient by introducing a correction matrix $\boldsymbol{L}$ to give

$$\tilde{\nabla} W_b(\boldsymbol{x}_a) = \boldsymbol{L}_a \nabla W_b(\boldsymbol{x}_a). \tag{42}$$

The velocity gradient is therefore evaluated now as

$$\nabla \boldsymbol{v}_a = \sum_{b=1}^{N} V_b(\boldsymbol{v}_b - \boldsymbol{v}_a) \otimes \tilde{\nabla} W_b(\boldsymbol{x}_a) = \sum_{b=1}^{N} V_b(\boldsymbol{v}_b - \boldsymbol{v}_a) \otimes \boldsymbol{L}_a \nabla W_b(\boldsymbol{x}_a). \tag{43}$$

The correction matrix $\boldsymbol{L}$ is obtained at each particle by enforcing that Eq. (41) is satisfied by the corrected kernel gradient. This gives

$$\sum_{b=1}^{N} V_b(\boldsymbol{x}_b - \boldsymbol{x}_a) \otimes \tilde{\nabla} W_b(\boldsymbol{x}_a) = \left(\sum_{b=1}^{N} V_b(\boldsymbol{x}_b - \boldsymbol{x}_a) \otimes \nabla W_b(\boldsymbol{x}_a) \right) \boldsymbol{L}_a^{\mathrm{T}} = \boldsymbol{I} \tag{44}$$

from which $\boldsymbol{L}$ is evaluated explicitly as

$$\boldsymbol{L}_a = \left(\sum_{b=1}^{N} V_b \nabla W_b(\boldsymbol{x}_a) \otimes (\boldsymbol{x}_b - \boldsymbol{x}_a) \right)^{-1}. \tag{45}$$

The use of this correction technique will ensure that the gradient of any linear velocity field is exactly evaluated. In addition, angular momentum will be preserved provided that the internal forces are derived from a variational principle.

4.2. Kernel correction

An alternative correction technique has been proposed by Liu [27,28] whereby the kernel itself is modified to ensure that polynomial functions up to a given degree are exactly interpolated. This is achieved by interpolating with a corrected kernel $\tilde{W}_b(\boldsymbol{x})$ as

$$\boldsymbol{v}(\boldsymbol{x}) = \sum_{b=1}^{N} V_b \boldsymbol{v}_b \tilde{W}_b(\boldsymbol{x}), \tag{46}$$

where for a first degree correction $\tilde{W}_b(\boldsymbol{x})$ is defined as

$$\tilde{W}_b(\boldsymbol{x}) = W_b(\boldsymbol{x}) \alpha(\boldsymbol{x}) [1 + \boldsymbol{\beta}(\boldsymbol{x}) \cdot (\boldsymbol{x} - \boldsymbol{x}_b)]. \tag{47}$$

The parameters $\alpha(\boldsymbol{x})$ and $\boldsymbol{\beta}(\boldsymbol{x})$ are evaluated by enforcing that any linear velocity distribution is exactly interpolated, that is,

$$\boldsymbol{v}_0 + \boldsymbol{v}_1 \cdot \boldsymbol{x} = \sum_{b=1}^{N} V_b(\boldsymbol{v}_0 + \boldsymbol{v}_1 \cdot \boldsymbol{x}_b)\tilde{W}_b(\boldsymbol{x}). \tag{48}$$

Since both $\boldsymbol{v}_0$ and $\boldsymbol{v}_1$ are arbitrary vectors, the following consistency conditions must therefore be satisfied by the corrected kernel,

$$\sum_{b=1}^{N} V_b \tilde{W}_b(\boldsymbol{x}) = 1, \tag{49}$$

$$\sum_{b=1}^{N} V_b(\boldsymbol{x} - \boldsymbol{x}_b)\tilde{W}_b(\boldsymbol{x}) = \boldsymbol{0}. \tag{50}$$

These equations enable the explicit evaluation of the correction parameters $\alpha(\boldsymbol{x})$ and $\boldsymbol{\beta}(\boldsymbol{x})$ as follows. Substituting Eq. (47) into Eq. (50) gives after simple algebra,

$$\boldsymbol{\beta}(\boldsymbol{x}) = \left[\sum_{b=1}^{N} V_b(\boldsymbol{x} - \boldsymbol{x}_b) \otimes (\boldsymbol{x} - \boldsymbol{x}_b) W_b(\boldsymbol{x})\right]^{-1} \sum_{b=1}^{N} V_b(\boldsymbol{x}_b - \boldsymbol{x}) W_b(\boldsymbol{x}). \tag{51}$$

Once $\boldsymbol{\beta}(\boldsymbol{x})$ has been evaluated the scalar parameter $\alpha(\boldsymbol{x})$ is obtained by substitution of Eq. (47) into Eq. (49) to give

$$\alpha(\boldsymbol{x}) = \frac{1}{\sum_{b=1}^{N} V_b[1 + \boldsymbol{\beta}(\boldsymbol{x}) \cdot (\boldsymbol{x} - \boldsymbol{x}_b)] W_b(\boldsymbol{x})}. \tag{52}$$

The use of this type of correction ensures that linear functions are perfectly interpolated and their gradients are exactly obtained. This ensures that condition (41), expressed now in terms of the corrected kernel, is satisfied. Note that this can be shown directly by taking the gradient Eq. (50).

The use of the above kernel correction is unsuitable for explicit type of calculations. This is due to the fact that the evaluation of the kernel gradient is cumbersome and computationally expensive as both $\alpha(\boldsymbol{x})$ and $\boldsymbol{\beta}(\boldsymbol{x})$ are functions of $\boldsymbol{x}$. A possible way of simplifying the calculation is by using constant, rather than linear, correction. This is equivalent to taking $\beta(\boldsymbol{x}) = \boldsymbol{0}$ in Eqs. (47) and (52) and leads to a weighted average or Shepard's interpolation of the velocity as

$$\boldsymbol{v}(\boldsymbol{x}) = \frac{\sum_{b=1}^{N} V_b \boldsymbol{v}_b W_b(\boldsymbol{x})}{\sum_{b=1}^{N} V_b W_b(\boldsymbol{x})}. \tag{53}$$

Note that the denominator in this expression is the parameter $\alpha(\boldsymbol{x})$. This interpolation leads to a far simpler evaluation of the kernel and velocity gradient but fails to satisfy the rotational invariance condition (41). Nevertheless, it provides a much improved interpolation, especially near the domain boundaries.

4.3. Mixed kernel and gradient correction

A final possible correction technique is achieved by combining the constant kernel correction shown in Eq. (53) with the gradient correction described in Section 4.1. For this purpose, the velocity approximation is expressed as

$$\boldsymbol{v}(\boldsymbol{x}) = \sum_{b=1}^{N} V_b \boldsymbol{v}_b \tilde{W}_b(\boldsymbol{x}), \quad \text{where } \tilde{W}_b(\boldsymbol{x}) = \frac{W_b(\boldsymbol{x})}{\sum_{b=1}^{N} V_b W_b(\boldsymbol{x})} \tag{54}$$

and the velocity gradient is evaluated as

$$\nabla \boldsymbol{v}_a = \sum_{b=1}^{N} V_b \boldsymbol{v}_b \otimes \tilde{\nabla} \tilde{W}_b(\boldsymbol{x}_a), \tag{55}$$

where the "corrected gradient of the corrected kernel" is defined as

$$\tilde{\nabla} \tilde{W}_b(\boldsymbol{x}_a) = \boldsymbol{L}_a \nabla \tilde{W}_b(\boldsymbol{x}_a). \tag{56}$$

Observe that the term $-\boldsymbol{v}_a$ is no longer required in Eq. (55) as the constant kernel correction already ensures that the gradient of constant function will vanish. Moreover, the gradient of the corrected kernel $\nabla \tilde{W}_b(\boldsymbol{x})$ can be easily evaluated by differentiation of Eq. (54) to give

$$\nabla \tilde{W}_b(\boldsymbol{x}) = \frac{\nabla W_b(\boldsymbol{x}) - \gamma(\boldsymbol{x})}{\sum_{b=1}^{N} V_b W_b(\boldsymbol{x})}, \quad \text{where } \gamma(\boldsymbol{x}) = \frac{\sum_{b=1}^{N} V_b \nabla W_b(\boldsymbol{x})}{\sum_{b=1}^{N} V_b W_b(\boldsymbol{x})}. \tag{57}$$

Additionally, enforcing Eq. (41), now in terms of the new corrected gradient $\tilde{\nabla} \tilde{W}_b(\boldsymbol{x}_a)$, yields an expression for the correction matrix as

$$\boldsymbol{L}_a = \left(\sum_{b=1}^{N} V_b \nabla \tilde{W}_b(\boldsymbol{x}_a) \otimes \boldsymbol{x}_b \right)^{-1}. \tag{58}$$

Finally, following the variational process outlined in Section 2 using Eq. (55) for the velocity gradient enables the internal equivalent forces for a given particle to be evaluated as

$$\boldsymbol{T}_a = \sum_{b=1}^{N} V_a V_b \boldsymbol{\sigma}_b \tilde{\nabla} \tilde{W}_a(\boldsymbol{x}_b). \tag{59}$$

5. Applications and examples

5.1. Introduction

In order to validate the present method three simple free-surface flow simulations, namely, a water bubble, the breaking of a dam and a bore, are presented in this paper. Computational results obtained are compared with theoretical solutions or experiment data. Also some of the additional numerical techniques used for free-surface flow computations are shown in this section.

5.1.1. Equation of state

The equation of state for liquids has been described by Batchelor [29] and the modified form proposed by Monaghan [13], which simulates sound waves accurately, is used herein. This equation of state can be written as

$$p = \kappa \left[\left(\frac{\rho}{\rho_0} \right)^{\gamma} - 1 \right], \tag{60}$$

where typically the value $\gamma = 7$ is used.

5.1.2. Time stepping

There are many possible forms of time integration methods which can be used to update the position of particles. The most common and simple time stepping scheme used in SPH literature are leap-frog explicit scheme [18] and the predictor–corrector scheme [20] which conserve linear and angular momentum exactly. To integrate the equilibrium equation using the leap-frog scheme, the intermediate velocities at point a are first found as

$$\boldsymbol{v}_a^{n+(1/2)} = \boldsymbol{v}_a^{n-(1/2)} + \overline{\Delta t} \boldsymbol{a}_a^n, \tag{61}$$

then the particle positions are updated as

$$\boldsymbol{x}_a^{n+1} = \boldsymbol{x}_a^n + \Delta t^{n+1} \boldsymbol{v}_a^{n+(1/2)}, \tag{62}$$

where $\overline{\Delta t} = \frac{1}{2}(\Delta t^n + \Delta t^{n+1})$ and $\boldsymbol{a}_a^n$ is the acceleration vector at point a computed using the equilibrium equation at step n.

Given the explicit nature of this time stepping method the Courant–Friedrichs–Lewy (CFL) stability requirement has to be satisfied. This implies that [21,22],

$$\Delta t = C_{\mathrm{FL}} \frac{h_{\min}}{\max_a(c_a + \|\boldsymbol{v}_a\|)}, \tag{63}$$

where $0 < C_{\mathrm{FL}} \leqslant 1$ is the Courant number and $c = \sqrt{\gamma\kappa/\rho}$ is the speed of sound.

Unfortunately, the use of the real bulk modulus for water in the equation of state would result in extremely small timesteps and therefore lengthy computations. In order to prevent this, an artificial smaller bulk modulus is typically used [13]. This is obtained by choosing a small ratio between the maximum speed of the fluid and the the speed of sound and then evaluating k as

$$k = c_{\max}^2 \rho/\gamma, \text{ where } c_{\max} = m\|\boldsymbol{v}\|_{\max}. \tag{64}$$

Values of m between 10 and 1000 are used.

5.2. Water bubble

In this section an elliptical water bubble flow simulation is presented [13]. This example is included to illustrate the capability of present method to accurately represent incompressible viscous free-surface flow, and to show that for the absence of external forces the total linear and angular momentum are preserved.

The geometry for the problem is a circle of 1 m radius with no external forces but with initial velocity field as $(-100x, 100y)$ m/s, (see Fig. 3). During the calculation the bubble should remain elliptical, the value of ab (semi-major axis $\times$ semi-minor axis) should remain constant and the outer boundary surface remain smooth. The domain is represented by 1184 randomly distributed particles with initial density $\rho = 10^3$ kg/m^3, viscosity $\mu = 0.5$ kg m^{-1} s^{-1} and artificial bulk modulus $\kappa = 285.714M$ N/m^2. The analytical solution of b varying with time can be analytically obtained as

$$\frac{\mathrm{d}b}{\mathrm{d}t} = -bB, \quad \text{where } \frac{\mathrm{d}B}{\mathrm{d}t} = \frac{B^2(b^4 - w^4)}{b^4 + w^4} \tag{65}$$

and w is the initial value of ab.

The above equations can be solved to high order of accuracy by using finite different methods and the results compared with both standard SPH and Corrected SPH simulations (CSPH). In Table 1, the values

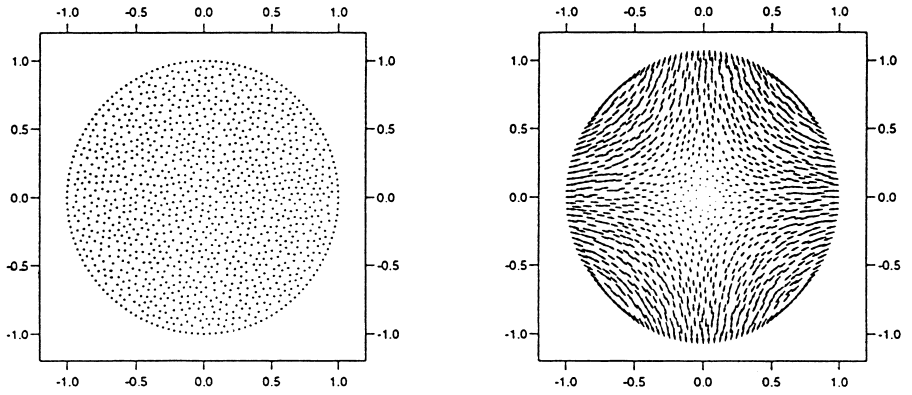

Fig. 3. Initial particle position and initial velocity field.

Table 1
Computational and theoretical values of b

Time (s)	Standard SPH	CSPH	Theory
0.002	1.22	1.22	1.22
0.005	1.61	1.60	1.60
0.008	2.02	2.00	2.00

of the semi-minor axis at different time step are shown. The maximum errors in the calculation for SPH and CSPH are less than 2% and less than 0.1%, respectively.

Figs. 4 and 5 show the particle position plotted at different time steps. The overall particle position in CSPH simulation is more uniformly distributed and the outer surface is far smoother than standard SPH method. Fig. 6 shows the total linear and angular momentum with time. Both methods preserve linear momentum exactly but only CSPH preserve angular momentum.

5.3. Breaking dam

The second example is a classic dam breaking flow simulation. A rectangular column of water, in hydrostatic equilibrium, is confined between the vertical wall and the gate, as shown in Fig. 7. The water column is 0.05715 m high and 0.05715 m wide. At time $t = 0$, the gate is removed instantaneously and the water is allowed to collapse under the force of gravity. Free-slip boundary conditions are implemented at the solid wall boundaries, with a gravitational acceleration of 9.81 m/s^2 acting vertically downwards. The density of water is 10^3 kg/m^3, and viscosity 0.5 kg m^{-1} s^{-1}. The mathematical model is represented by 2916 particles. The value of artificial bulk modulus is computed as

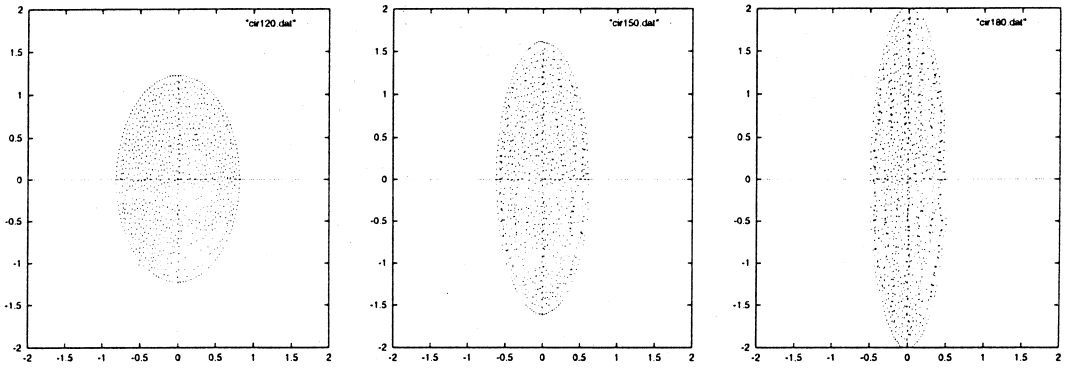

Fig. 4. Standard SPH method.

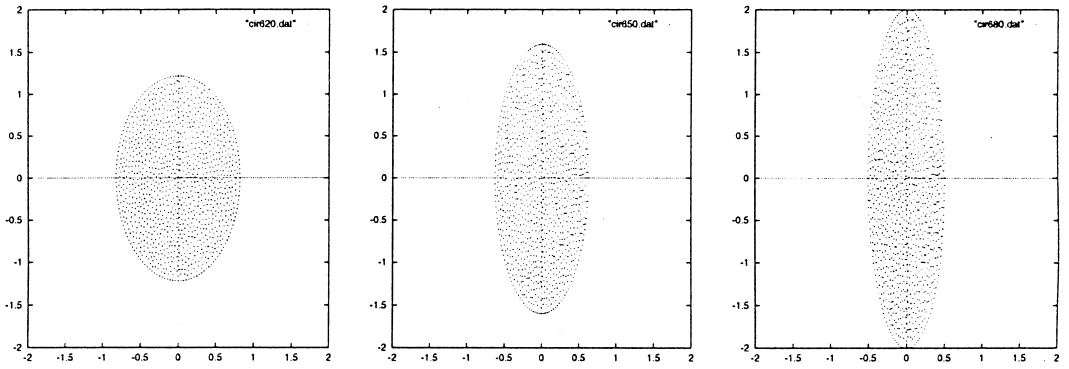

Fig. 5. Mixed kernel and gradient corrected method.

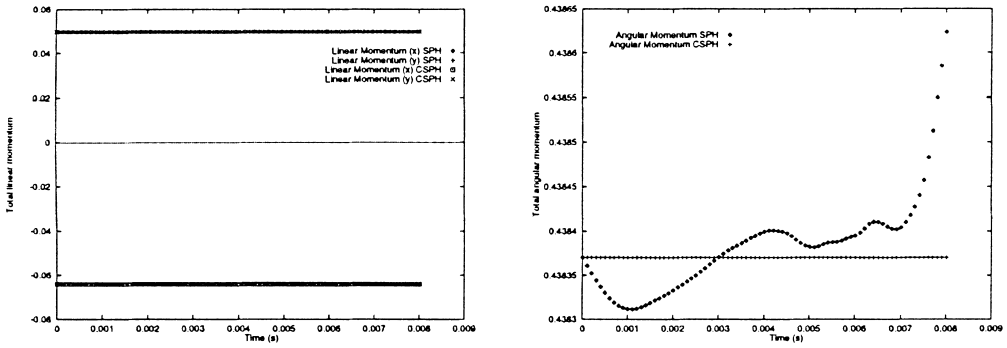

Fig. 6. Total linear momentum (left) and total angular momentum (right).

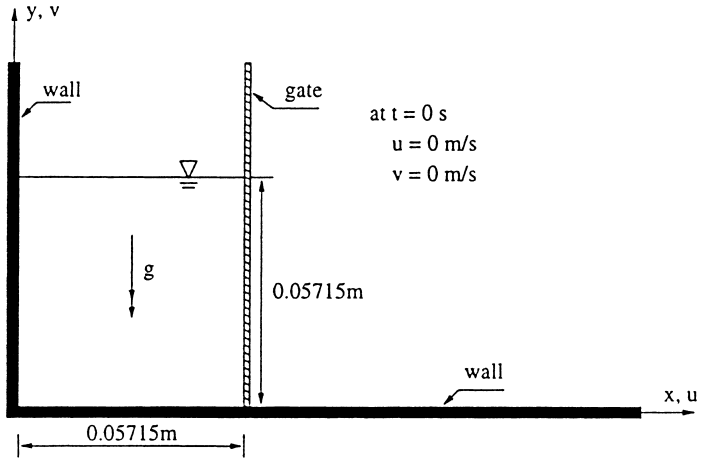

Fig. 7. Schematic diagram of the broken dam problem.

$$\kappa = \frac{100(2gh)\rho}{\gamma}, \tag{66}$$

where $2gh$ is the upper bound speed and h is the height of the dam.

Fig. 8 shows a comparison of the numerical results obtained against experimental data by Martin and Moyce [30]. For convenience, all the variables used in the computation are non-dimensionalised by choosing the initial width of the dam a as a reference length, from which the dimensionless time and surge front positions are defined as $t\sqrt{g/a}$ and z/a, where g is the gravitational acceleration and z is surge front. The results obtained from CSPH method are approximately 5% away from the published experimentally obtained data.

Fig. 9 shows the particle configurations for the collapsing dam at representative times using standard SPH. The same results obtained mixing equilibrium Eq. (8) with density Eq. (1) is shown in Fig. 10. Finally the result obtained using mixed kernel and gradient CSPH method is illustrated in Fig. 11. It is worth noting the poor results obtained using variationally inconsistent density and force equations as shown in Fig. 10.

5.4. Bore

One advantage of using a Lagrangian meshless based formulation to solve fluid flow problems is its ability to deal with highly unsteady situations. In order to illustrate this capability, consider a calculation of a bore simulation. The moving bore is a well-studied type of flow [31–33] for which a simplified analytical

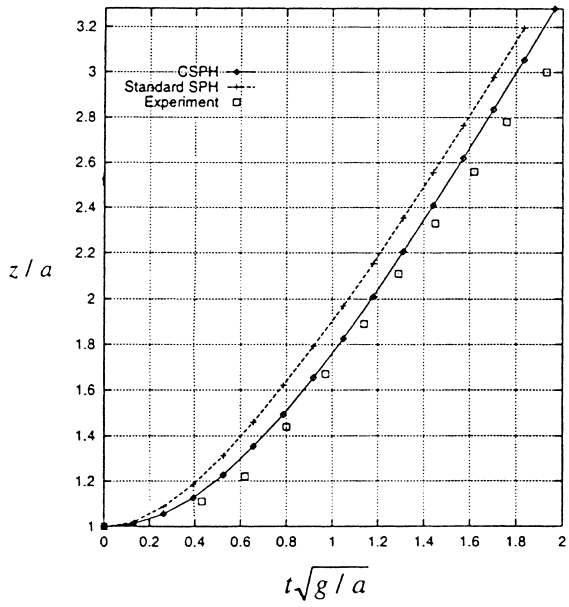

Fig. 8. Comparison of computational and experimental results of surge front location.

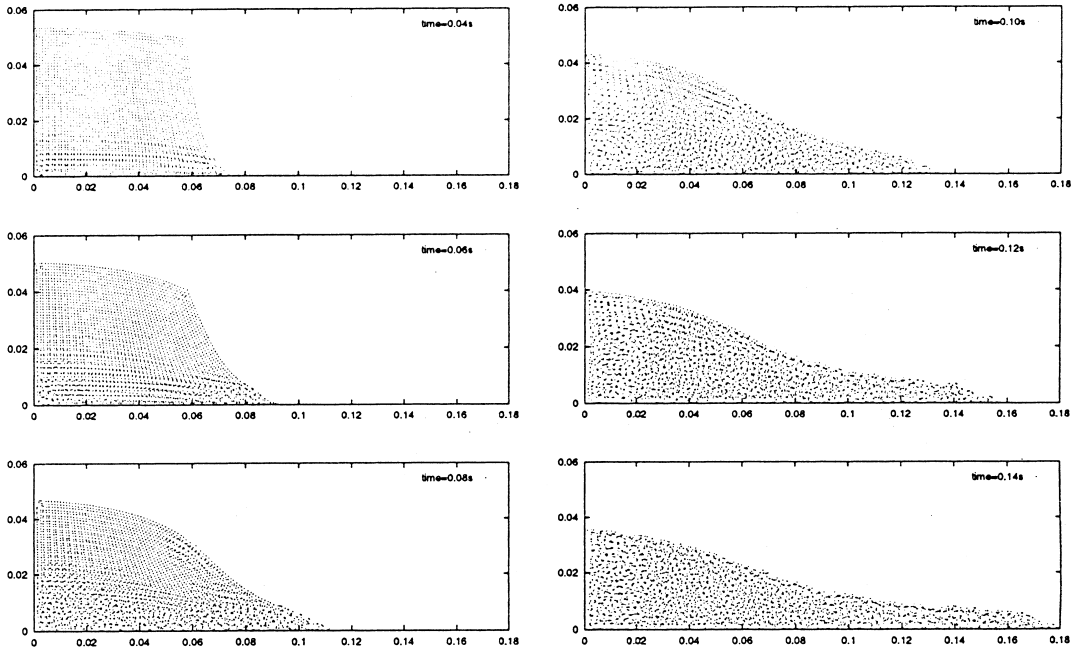

Fig. 9. Particle position plots for broken dam problem using standard SPH method.

solution is available. Fig. 12 shows a horizontal layer of water being pushed into a rigid, vertical wall, resulting in a hydraulic jump or bore being produced that runs away from the wall, where v_0 is the initial velocity, v_s is the speed of the bore, h_0 and h are the initial height and bore height.

If g, h_0 and v_0 are known, v_s and h can be computed by using

$$v_s = -v_0 + \sqrt{\tfrac{1}{2}gh(1 + h/h_0)}, \tag{67}$$

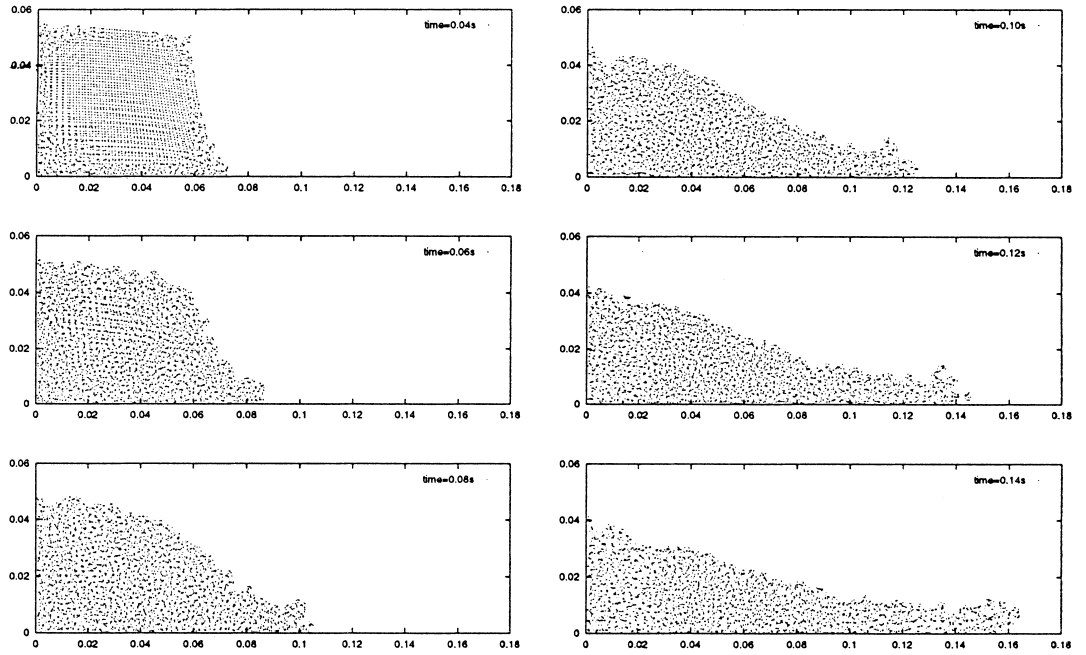

Fig. 10. Particle position plots for broken dam problem using Eq. (8) mixed with Eq. (1).

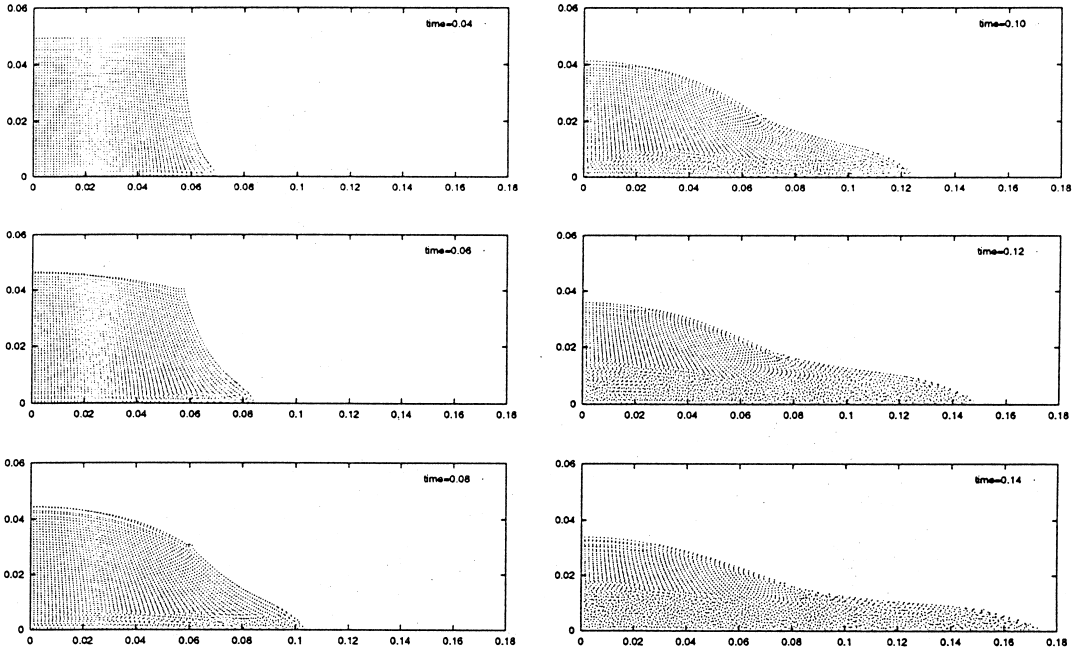

Fig. 11. Particle position plots for broken dam problem: mixed kernel and gradient CSPH.

together with

$$\frac{h}{h_0} = \frac{v_s + v_0}{v_s}. \tag{68}$$

In this problem, CSPH was used to compute the bore evolution, and two cases with different initial velocity set-ups were studied. The initial configuration of this problem is a rectangular water column 0.1 m in height

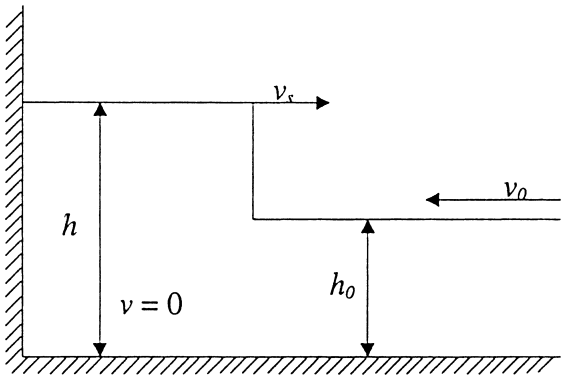

Fig. 12. The configuration of an idealised bore.

and 1.5 m wide. The domain is represented by 6321 particles, with initial density 10^3 kg/m^3, viscosity 0.001 kg m^{-1} s^{-1}, initial velocities of 0.2971 m s^{-1} or 0.9813 m s^{-1} (giving Froude numbers 0.3 and 0.9 respectively). Free-slip boundary conditions are implemented at the solid wall boundaries and push-wall boundary conditions are used at the right hand side of the water column.

Figs. 13 and 14 show the fluid configuration of a bore. At low speed the wave is so small that a broken wave front does not form, and instead an unbroken wave travels to the right, giving the so-called "undulant jump" configuration. In the second case when the water column travels at high speed and there is a splash

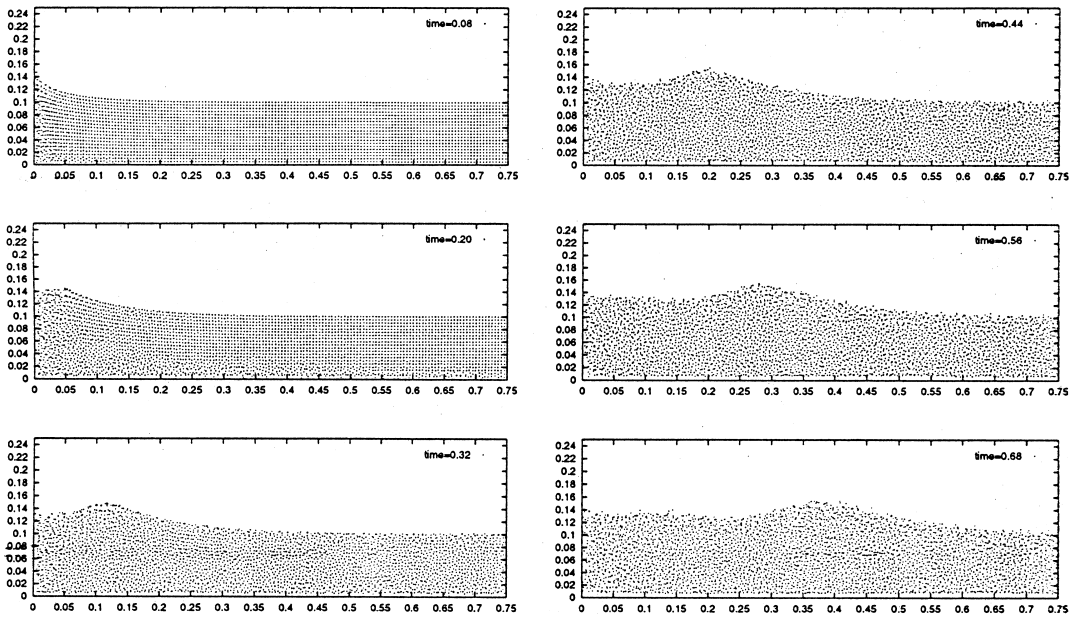

Fig. 13. The hydraulic jump simulation with initial velocity 0.2971 m s^{-1}.

Table 2
Computational and theoretical values of bore height and speed of case 2

	Time (s)				Mean	Theory	Error (%)
	0.48	0.52	0.56	0.60			
Height (m)	0.1980	0.2016	0.1968	0.2004	0.1992	0.2043	2.50
Velocity (m s^{-1})	0.8994	0.8500	0.8688	0.8381	0.8641	0.8546	1.11

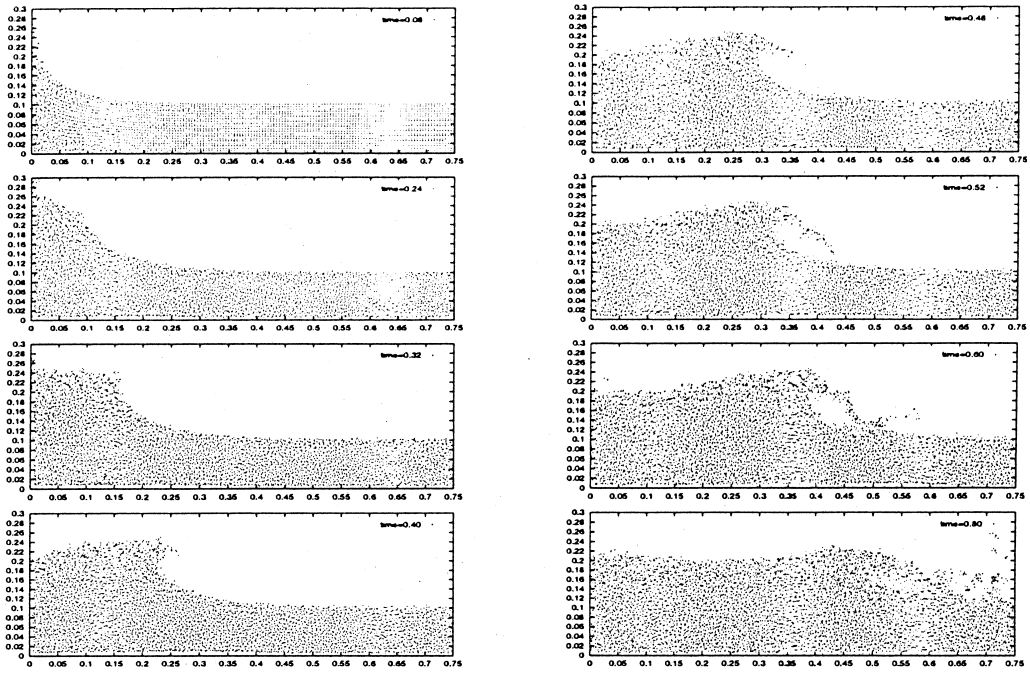

Fig. 14. The hydraulic jump simulation with initial velocity 0.9813 m s^{-1}.

of water surge up the wall and the front of the bore becomes a wave breaker. Table 2 presents the obtained results from computer simulation compared with theoretical solutions, the error is less than 3%.

6. Concluding remarks

This paper has discussed the variational implications of alternative SPH equations commonly used in the literature. The examples shown illustrate the benefits of using pairs of density and force equations that are variationally consistent. The paper has also presented the conditions that must be satisfied by the force equations in order to ensure that in the absence of external forces linear and angular momentum are preserved. Experience in other fields of dynamic computer simulations has shown that preservation of momentum is a common feature of well-behaved and accurate algorithms. Several correction techniques have been presented in the paper in order to improve the accuracy of the SPH algorithms. The improvements observed are illustrated with a number of examples in the area of free surface water flow. These type of applications with simple physics but complex flows provide are ideal for testing and exploiting the advantages of mesh fee methods such as SPH or corrected SPH algorithms.

Acknowledgements

The authors wish to thank Dr. R.F. Allen for his advice and efforts in carrying out the experiment of the bore example in the fluid laboratory of Civil Engineering Department, University of Wales Swansea and Mr. S. Kulasageram for his interest, encouragement and numerous useful discussions. This research has been partly funded by EPSRC via contracts GR/K77631 and GR/L78352.

References

[1] L.B. Lucy, A numerical approach to the testing of the fission hypothesis, Astro. J. 82 (1977) 1013.
[2] R.A. Gingold, J.J. Monaghan, SPH: Theory and application to non-spherical stars, Mon. Not. R. Astron. Soc. 181 (1977) 375.

[3] M. Schussler, D. Schmitt, Comments on SPH, Astron. Astrophys. 97 (1981) 373.
[4] R.A. Gingold, J.J. Monaghan, Kernel estimates as a basis for general particle methods in hydrodynamics, J. Comput. Phys. 46 (1982) 429.
[5] T. Belytschko, Feature articles: Are finite elements passe, ISACM Bulletin 7 (1994) 4.
[6] L.D. Libersky, A.G. Petschek, T.C. Carney, J.R. Hipp, F.A. Allahdadi, High strain Lagrangian hydrodynamics, J. Comput. Phys. 109 (1993) 67.
[7] A.G. Petschek, L.D. Libersky, Cylindrical SPH, J. Comput. Phys. 109 (1993) 76.
[8] G.R. Johnson, E.H. Petersen, R.A. Stryk, Incorporation of an SPH option into the epic code for a wide range of high velocity impact computations, Int. J. Impact Engng. 14 (1993) 385.
[9] R.F. Stellingwerf, C.A. Wingate, Impact modelling with SPH, Int. J. Impact Engng. 14 (1993) 707.
[10] W. Benz, E. Asphaug, Simulations of brittle solids using SPH, Comput. Phys. Comm. 87 (1995) 253.
[11] G.R. Johnson, R.A. Stryk, S.R. Beissell, SPH for high velocity impact computations, Comput. Meth. Appl. Mech. Engng. 139 (1996) 347.
[12] G.R. Johnson, S.R. Beissel, Normalised smoothing functions for SPH impact computations, Int. J. Num. Meth. Engng. 39 (1996) 2725.
[13] J.J. Monaghan, Simulating free surface flows with SPH, J. Comp. Phys. 110 (1994) 399.
[14] H. Takeda, S.M. Miyama, M. Sekiya, Numerical simulation of viscous flow by SPH, Prog. Theor. Phys. 92 (1994) 939.
[15] J.J. Monaghan, A. Kocharyan, SPH simulation of multi-phase flow, Comput. Phys. Comm. 87 (1995) 225.
[16] J.P. Morris, P.J. Fox, Y. Zhu, Modelling low reynolds number incompressible flows using SPH, J. Comp. Phys. 136 (1997) 214.
[17] J.J. Monaghan, Why particle methods work, SIAM J. Sci. Stat. Comput. 3 (1982) 422.
[18] J.J. Monaghan, Particle methods for hydrodynamics, Comput. Phys. Reports 3 (1985) 71.
[19] J.J. Monaghan, An introduction to SPH, Comput. Phys. Comm. 48 (1988) 89.
[20] J.J. Monaghan, On the problem of penetration in particle methods, J. Comp. Phys. 82 (1989) 1.
[21] J.J. Monaghan, SPH, Annu. Rev. Astron. Astrophys. 30 (1992) 543.
[22] P.W. Randles, L.D. Libersky, SPH: Some recent improvements and applications, Comput. Methods Appl. Mech. Engng. 139 (1996) 375.
[23] B. Hassani, J. Bonet, CSPH, Department of Civil Engng., University of Wales Swansea, Internal Report CR/900/97, 1997.
[24] J. Bonet, B. Hassani, T.S.L. Lok, S. Kulasageram, CSPH – A Reproducing Kernel Meshless Method for Computational Mechanics, 5th ACME-UK conference, London, 1997.
[25] T.S.L. Lok, J. Bonet, CSPH Method for Viscous Free-Surface Flow, 6th ACME-UK conference, Exeter, 1998.
[26] J. Bonet, R.D. Wood, Non-linear Continuum Mechanics for Finite Element Analysis, Cambridge University Press, Cambridge, UK, 1997.
[27] S.F. Li, W.K. Liu, Moving least square Kernel Galerkin method (II) Fourier analysis, Comput. Methods Appl. Mech. Engng. 139 (1996) 159.
[28] W.K. Liu, S.F. Li, T. Belytschko, Moving least square Kernel Galerkin method (I) methodology and convergence, Comput. Methods Appl. Mech. Engng. 143 (1997) 113.
[29] G.K. Batchelor, An Introduction to Fluid Dynamics, Cambridge University Press, Cambridge, UK, 1967.
[30] J.C. Martin, W.J. Moyce, Part IV. An experimental study of the collapse of liquid columns on a rigid horizontal plane, Phil. Tran. R. Soc. London 244 (1952) 312.
[31] F.M. Henderson, Open Channel Flow, Collier–Macmillan Publishing Company, London, 1966.
[32] J.J. Stoker, Water Waves: The Mathematical Theory with Applications, Interscience Publishers, New York, 1957.
[33] F.H. Harlow, A.A. Amsden, Fluid dynamics: An introductory text, Los Alamos Sci. Lab., LA-4100, 1970.